GEOLOGY

Long-term magmatic evolution reveals the beginning of a new caldera cycle at Campi Flegrei

Francesca Forni[1]*, Wim Degruyter[2], Olivier Bachmann[1], Gianfilippo De Astis[3], Silvio Mollo[3,4]

Understanding the mechanisms that control the accumulation of large silicic magma bodies in the upper crust is key to determining the potential of volcanoes to form caldera-forming eruptions. Located in one of the most populated regions on Earth, Camp Flegrei is an active and restless volcano that has produced two cataclysmic caldera-forming eruptions and numerous smaller eruptive events over the past 60,000 years. Here, we combine the results of an extensive petrological survey with a thermomechanical model to investigate how the magmatic system shifts from frequent, small eruptions to large caldera-forming events. Our data reveal that the most recent eruption of Monte Nuovo is characterized by highly differentiated magmas akin to those that fed the pre-caldera activity and the initial phases of the caldera-forming eruptions. We suggest that this eruption is an expression of a state shift in magma storage conditions, whereby substantial amounts of volatiles start to exsolve in the shallow reservoir. The presence of an exsolved gas phase has fundamental consequences for the physical properties of the reservoir and may indicate that a large magma body is currently accumulating underneath Campi Flegrei.

INTRODUCTION

Caldera-forming magmatic systems often follow recurrent evolutionary paths [i.e., caldera cycles (*1*)] accompanied by notable changes in the composition and physical properties of erupted magmas, frequency, spatial distribution and size of volcanic eruptions, and architecture of the magmatic reservoir at depth [e.g., Kos-Nisyros volcanic complex (*2*), Taupo Volcano (*3*), Katla (*4*), Valles caldera (*5*), and Santorini (*6*)]. Caldera cycles typically start with a build-up stage, during which silicic magmas incrementally accumulate in a thermally mature upper crustal reservoir. This stage, which is characterized by few relatively small eruptions of differentiated magmas and long dormancy episodes, culminates in a climactic eruption associated with large-scale magma withdrawal and caldera collapse. Subsequently, during the post-collapse stage, recharge of deeper magmas in a largely emptied and crystallized shallow reservoir leads to small and more frequent eruptions of less differentiated compositions (often generating surface resurgence). These compositions can potentially evolve toward more silicic and volatile-rich end members, starting a new cycle.

Over the past decades, many efforts have been devoted to the study of caldera-forming eruptions because of their critical impact on life on our planet (*7*–*12*), but less attention has been dedicated to the analysis of the evolutionary stages that lead to the accumulation of these large volumes of silicic magmas in the upper crust. A better understanding of the geologic significance of the sequence of events that culminates in high-magnitude volcanic eruptions is crucial to get information about the past and present of active calderas as key to forecast their future behavior.

Home to more than 1.5 million people, the Campi Flegrei caldera (Southern Italy) represents one of the most hazardous regions on Earth, and its magmatic history has been the focus of a number of studies (*8*, *13*–*21*). Notably, two large-volume caldera-forming eruptions [Campanian Ignimbrite (CI), ~39 thousand years (ka) ago and Neapolitan Yellow Tuff (NYT), ~15 ka ago] and a vast number of smaller volcanic events occurred at Campi Flegrei in the past 60 ka. Since the last historical eruption (Monte Nuovo, 1538 AD), the caldera has gone through recurrent episodes of unrest, suggesting that the magmatic system is active and potentially prone to erupt again in the future (*22*, *23*). Because most of the previous studies focused only on a single eruption or a specific period of activity, key aspects about the long-term magmatic evolution of Campi Flegrei are still poorly understood.

Here, we combine textural information with major and trace element compositions of bulk rock, mineral, and glass samples from 23 eruptions at Campi Flegrei, including the two caldera-forming events (CI and NYT) and key units representative of the pre- and post-caldera activities (pre-CI, post-CI/pre-NYT, and post-NYT; Fig. 1 and Supplementary Materials). Using thermometers and hygrometers specifically calibrated to alkaline compositions akin to the Phlegraean magmas (*24*, *25*), we estimate the time paths of magmatic temperature and water content through the eruptive history of Campi Flegrei. Last, we use a thermomechanical reservoir model (*26*) to investigate the 15-ka long period of activity that followed the NYT eruption to get insights into the recent behavior and present status of the Campi Flegrei magmatic system.

RESULTS

Geochemical and textural characteristics of erupted magmas

Our petrological data show that the first caldera-forming eruption at Campi Flegrei, the CI, is characterized by a zoned sequence that starts with crystal-poor and highly evolved magmas [≤6% crystals; differentiation index (DI) = 86 to 91] and transitions into more crystalline and less evolved material (36 to 37% crystals; DI = 75 to 85; Fig. 1). The second caldera-forming unit, the NYT, is overall relatively crystal-poor (≤10% crystals) and compositionally heterogeneous (DI = 70 to 88), with the less evolved material becoming more abundant during the final eruptive stages (Fig. 1). The highly evolved magmas of both CI and NYT mostly contain low Sr-Ba matrix glass with negative Eu anomalies (Fig. 2) and mineral phases in equilibrium with the host melt (e.g., low Sr-Ba sanidines, type 2; Fig. 3). Conversely, the less evolved material encloses chemically zoned crystals [i.e., zoned sanidines showing a sharp increase in Sr and Ba toward crystal rims (type 1) and clinopyroxene with positive Eu anomalies (type 2); Fig. 3 and fig. S3, respectively] and matrix glass compositions with relatively high Ba and Sr contents

[1]Institute of Geochemistry and Petrology, ETH Zürich, Clausiusstrasse 25, 8092 Zürich, Switzerland. [2]School of Earth and Ocean Sciences, Cardiff University, Park Place, Cardiff CF10 3AT, Wales, UK. [3]Istituto Nazionale di Geofisica e Vulcanologia, via di Vigna Murata 605, 00143 Roma, Italy. [4]Dipartimento di Scienze della Terra, Sapienza-Università di Roma, P.le Aldo Moro 5, 00185 Roma, Italy.
*Corresponding author. Email: francesca.forni05@gmail.com

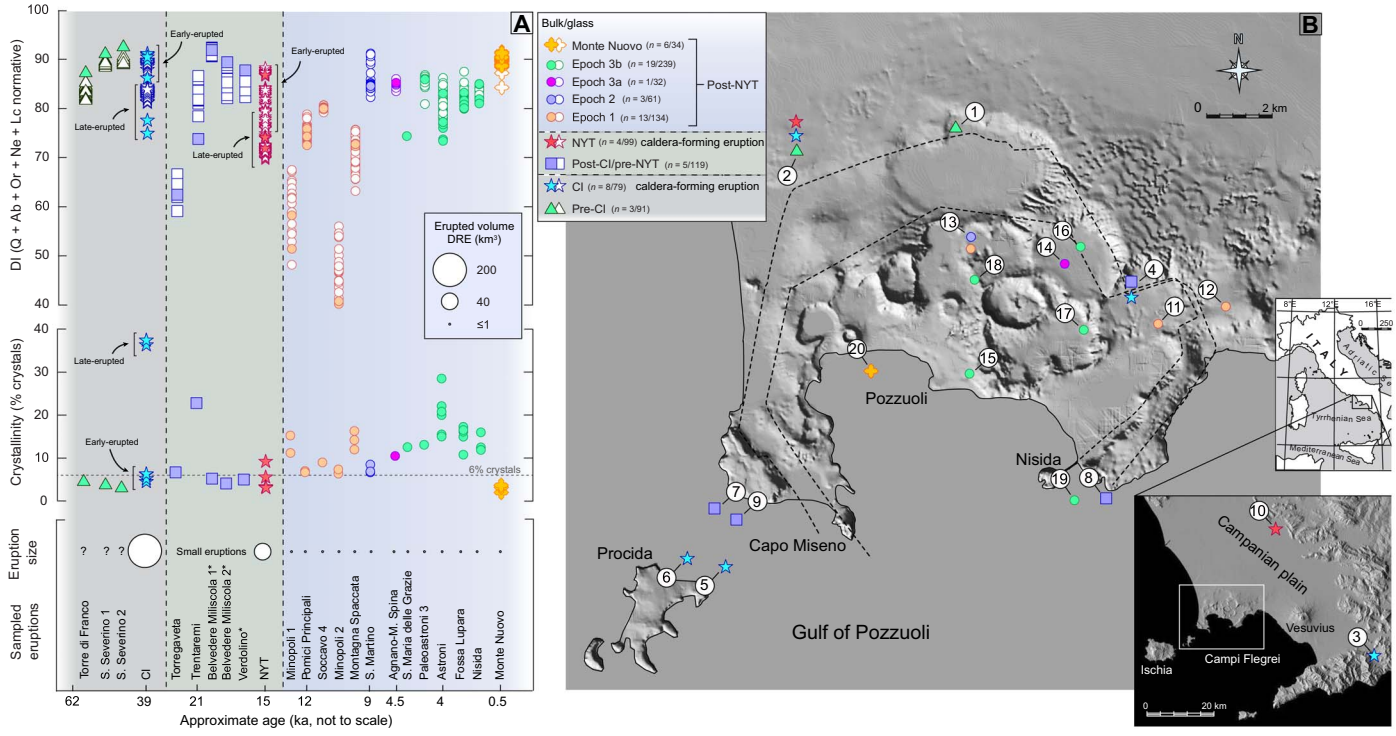

Fig. 1. Studied units and sampling localities. (**A**) Variation in time of magma DI (DI = Q + Ab + Or + Ne + Lc normative), crystallinity (% crystals), and eruption size for the sampled eruptions. The calculated crystallinity exclusively accounts for the amount of macrocrysts. The groundmass crystallinity was calculated and subtracted from the total crystallinity when microlites were observed (see Materials and Methods). Approximate ages and relative stratigraphic position of the sampled units were compiled using data from the literature (see the Supplementary Materials). About 200 and 40 km^3 of magma dense rock equivalent (DRE) were erupted during the CI (*15*) and the NYT (*21*), respectively. The volume of the pre- and post-caldera eruptions is not very well constrained because of the paucity of preserved outcrops. The available field data and drill-hole observations suggest that the post-CI/pre-NYT activity mostly consisted of small-volume eruptions (*69*). During the post-NYT activity, the erupted volumes were generally less than 0.1 km^3 (although some reached up to 1 km^3 DRE). Bulk rock data are reported on anhydrous basis. Fe_2O_3 was converted to FeO (= Fe_2O_3 × 0.8998) to compare bulk rock data with the matrix glass compositions. Asterisks indicate the units with uncertain relative stratigraphic position (see the Supplementary Materials). In the legend, *n* denotes the number of bulk rock (*x*) and glass (*y*) analyses. (**B**) Shaded relief map of Campi Flegrei caldera and Campanian Plain showing the sampling localities (numbers correspond to the sites reported in the data file S1). The dashed lines indicate the reconstructed CI and NYT caldera rims (*70*). A simplified map shows the location of the study area in Southern Italy.

and positive Eu anomalies (Fig. 2), which suggests complex magma interactions including mixing and partial remelting of cumulate material (*27*, *28*).

After the caldera-forming eruptions, basaltic trachyandesites and trachyandesites (6 to 16% crystals; DI = 40 to 74), evolving toward trachyphonolites (6 to 28% crystals; DI = 74 to 92), were emitted (Fig. 1). The least evolved magmas bear olivine and unzoned sanidines (type 2), whereas the intermediate and evolved ones contain K-feldspars with high Ba-Sr rims (type 1; Fig. 3). Notably, increasing Eu anomalies toward clinopyroxene rims (type 5; fig. S3) are recognized in the post-CI/pre-NYT and post-NYT crystal-rich units (12 to 28% crystals).

The last eruption at Monte Nuovo is characterized by particularly homogeneous, evolved, and crystal-poor magmas (≤ 3% crystals; DI = 84 to 91), resembling those that were erupted during the initial phases of caldera-forming events. Matrix glass compositions show low Ba and Sr contents and negative Eu anomalies (Fig. 2). Unzoned sanidine with low Sr and Ba contents (type 2; Fig. 3) and normally zoned clinopyroxene (types 1 and 3; fig. S3) represent the most common mineral phases. Magmas with similar petrological characteristics were also erupted at Campi Flegrei during the pre-caldera phases of activity (Fig. 1) and are reported for some post-NYT eruptions [Fondi di Baia and Averno 2; (*20*, *29*)] (fig. S1).

Cycles in magma temperature and water content

Variations of crystallization temperatures and magma water contents through time estimated for the investigated eruptions at Campi Flegrei define cyclic paths leading toward a gradual decrease of temperature and increase of water content before the two caldera-forming eruptions and the most recent eruption of Monte Nuovo (Fig. 4). Specifically, the highly evolved and crystal-poor pre-CI units show decreasing equilibrium temperatures (from ~990° to 870°C) and increasing water contents [from ~4 to 7 weight % (wt %)] before the caldera-forming eruption (Fig. 4). The CI records a wide range of temperatures and water contents (Fig. 4), with the crystal-poor and evolved subunits being colder and drier (~880° to 970°C and ~4 to 6 wt % H_2O) than the crystal-rich subunits (~950° to 1050°C and ~3 to 5 wt % H_2O). Eruption of more mafic, hotter, and drier magmas (~1000° to 1090°C and ~3 to 5 wt % H_2O) progressing in time through intermediate (~930° to 1070°C and ~4 to 6 wt % H_2O) and finally evolved, colder, and water-rich melts (~880° to 930°C and 5 to 7 wt % H_2O) follow the CI and precede the NYT eruption (Fig. 4). Similar to the CI, the NYT spans a continuous range of temperatures and water contents, from the relatively cold, wet, and evolved compositions to the hotter, drier, and less differentiated magmas (~900° to 1070°C and ~3 to 6 wt % H_2O). Immediately after the NYT (epoch 1), we find again more mafic and hotter

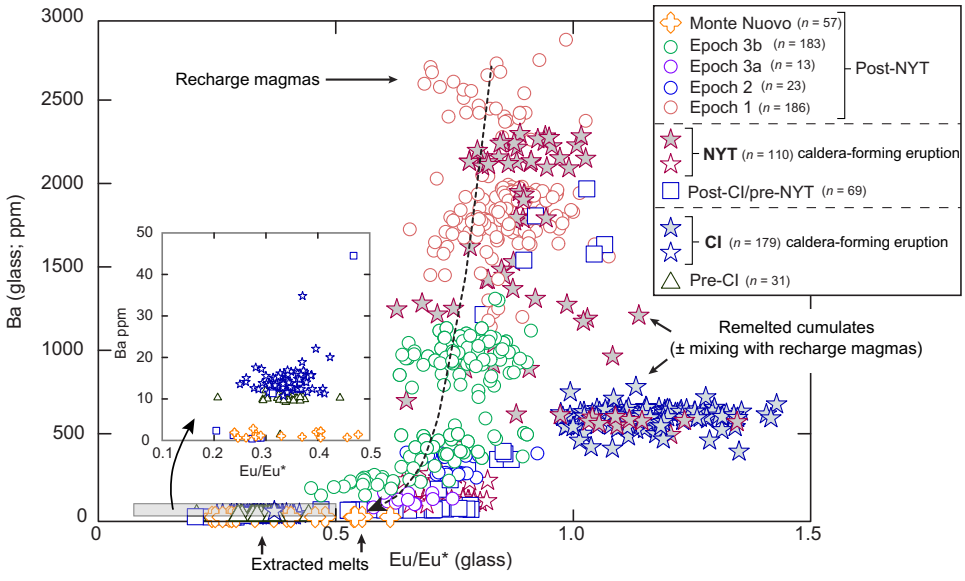

Fig. 2. Matrix glass compositions. Plot of Eu anomaly [$Eu/Eu^* = Eu_N/(Sm_N \times Gd_N)^{1/2}$; trace element concentrations normalized to values from (*71*)] versus Ba content [in parts per million (ppm)] in matrix glasses from the sampled eruptions at Campi Flegrei. The low Ba-Eu/Eu* region of the plot is enlarged in the inset. In the CI and NYT, white-filled symbols refer to the most evolved compositions, whereas gray-filled symbols refer to the least evolved and predominantly late-erupted compositions (see Fig. 1). Note that the fractional crystallization of a feldspar-dominated mineral assemblage drives the residual liquid toward progressive depletion in Ba, Eu/Eu* (dashed arrow), and Sr. A combined effect of fractional crystallization and crystal-liquid separation produces extracted melts with much higher fractionated geochemical signatures compared to those obtained by simple fractional crystallization (*27*). This explains why the highly evolved matrix glass compositions (i.e., extracted melts) belong to the crystal-poor units (e.g., pre-CI, early phases of CI, pre-NYT, and Monte Nuovo). Matrix glasses displaying intermediate Ba (and Sr) together with positive Eu anomalies in the caldera-forming units are interpreted as representative of the liquids derived by remelting of a feldspar-dominated cumulate mush (i.e., remelted cumulates) (*34*). Typical uncertainty (1σ) is smaller than the size of symbols. In the legend, *n* denotes the number of glass analyses.

magmas (~1020° to 1130°C) gradually progressing toward more evolved and colder conditions (Fig. 4). Subsequently (epochs 2 and 3), only more evolved magmas showing lower temperatures (~900° to 1080°C) and higher water contents (~3 to 6 wt % H_2O) were emitted (Fig. 4). The last eruption at Monte Nuovo marks an increase of magma water content (~5 to 7 wt % H_2O) coupled with a notable decrease of the crystallinity (~2 to 3 wt % crystals) and temperature (~870° to 920°C) of erupted magmas (Fig. 4).

DISCUSSION

Evolution of the magmatic system through time

The compositional variations displayed by the Phlegraean magmas describe an alkaline differentiation trend from basaltic trachyandesites to trachyphonolites (fig. S2). A number of geochemical and isotopic investigations suggest that this evolutionary trend is largely controlled by fractional crystallization processes occurring at multiple crustal levels with minor crustal assimilation and mixing [e.g., (*15*, *30*)]. Crystal-liquid separation involves mainly sanidine and plagioclase together with clinopyroxene, biotite, and Fe-Ti oxides, leading to the development of feldspar-dominated cumulate mushes (*31*). In this environment, melt extraction from crystalline magma reservoirs, which occurs most efficiently at intermediate crystallinity stage [50 to 70% crystals (*32*)], promotes the aggregation of lenses of highly differentiated, crystal-poor, and volatile-rich magmas in the upper part of the magma chamber (*33*). Our data show that magmas with these physicochemical characteristics were erupted at Campi Flegrei, immediately before and during the initial phases of caldera-forming eruptions (Figs. 1 and 4). The negative Eu anomalies and low Sr-Ba contents measured in matrix glasses (Fig. 2) and mineral phases (Fig. 3 and fig. S3) suggest that these magmas

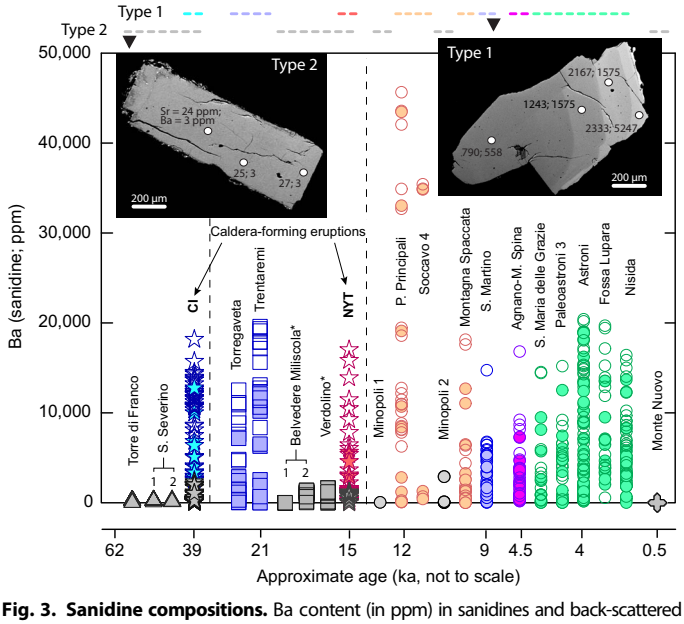

Fig. 3. Sanidine compositions. Ba content (in ppm) in sanidines and back-scattered images of the two types of crystals recognized in the studied units (asterisks indicate the units with uncertain relative stratigraphic position; see the Supplementary Materials). Solid symbols refer to crystal cores, whereas empty symbols refer to crystal rims. Type 1 crystals are zoned and show increasing Sr and Ba contents toward crystal rims (colored symbols). Type 2 crystals are unzoned and show low Sr and Ba contents (gray symbols). Dashed lines indicate the occurrence of type 1 (colored lines) and type 2 (gray lines) crystals in the studied units. Note that only the two caldera-forming eruptions contain both types of sanidine. Typical uncertainty (1σ) is smaller than the size of symbols. Number of sanidine analyses (*n*): 87 (pre-CI), 181 (CI), 141 (post-CI/pre-NYT), 71 (NYT), 85 (epoch 1), 37 (epoch 2), 44 (epoch 3a), 220 (epoch 3b), and 98 (Monte Nuovo).

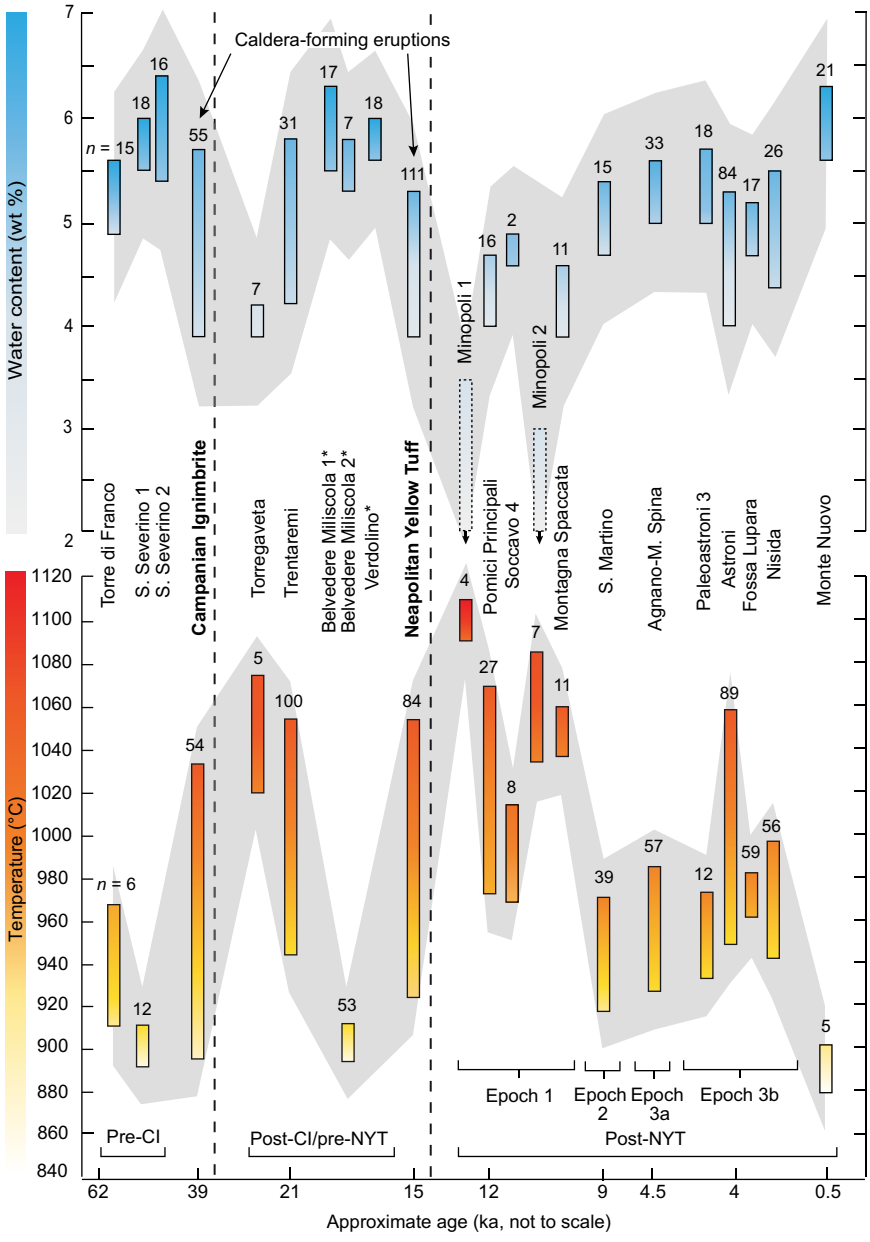

Fig. 4. Variations of temperature and water content. Time paths of equilibrium temperature (°C) and magma water content (wt %) estimated for the studied units (asterisks indicate the units with uncertain relative stratigraphic position; see the Supplementary Materials) using clinopyroxene-liquid thermometry (*24*) and K-feldspar–liquid hygrometry (*25*). *n* indicates the number of mineral-liquid equilibrium couples. Note that no clinopyroxene-liquid equilibrium pairs were obtained for S. Severino 2, Belvedere Miliscola 1, and Verdolino and that no K-feldspars–liquid equilibrium pairs were obtained for Minopoli 1 and 2. Water contents obtained via melt inclusion analyses from the literature (dashed bars) are reported for these two units [1 to 3.5 ± 0.4 wt % (*55*) and 0.2 to 3 ± 0.5 wt % (*56*), respectively]. The gray area includes the errors of estimate associated with the clinopyroxene-liquid thermometer (±20°C) and K-feldspar–liquid hygrometer (±0.7 wt %). See Materials and Methods.

are representative of the residual melts extracted from a crystal mush system after substantial feldspar fractionation.

Portions of cumulate mush can be reactivated by partial melting of low-temperature mineral phases (e.g., feldspars), following hotter recharge (*34*). This process is essential to reduce the crystallinity of the cumulate mush, making it rheologically eruptible (<50% crystals), and typically produces relatively hot and dry melts, locally enriched in Sr, Ba, and Eu/Eu* (*35*). We found strong evidence of these melts in the composition of matrix glasses (Fig. 2) and minerals (Fig. 3 and figs. S3 to S5) from the CI and the NYT. Hence, during the caldera-forming eruptions at Campi Flegrei, both highly differentiated, relatively cold, and water-rich extracted melts and less evolved, hotter, and drier magmas (representing remobilized portions of the cumulate mush) were erupted, generating zoned ignimbrites (caldera stage; Fig. 5A). Notably, a clear distinction between crystal-poor and crystal-rich subunits, representing the segregated melts and remobilized portions of the cumulate mush, respectively, is observed in the CI (*27*). Conversely, the NYT magmas are dominantly crystal poor and span a wider compositional range than the one recorded in the CI juvenile clast (Figs. 1 and 2). The most mafic compositions

of the NYT are characteristic of the invading magma that triggered cumulate melting and mixed with the resident evolved melts (*28*). These mafic compositions are much less obvious in the CI, where these signatures have been diluted by the higher volumes of evolved resident magmas (*36*).

While the eruptible portion of the upper crustal magma reservoir was evacuated during the caldera-forming eruptions leading to caldera collapse, volumes of residual mush likely remained in the crust (*31*). As this remaining mush was likely gas saturated, depressurization during caldera collapse led to massive devolatilization and associated crystallization. Subsequently, ascent of more mafic and hotter magmas of deeper origin could not easily stop in the stiffer upper crustal reservoir, favoring eruption along the newly formed caldera ring faults and the regional faults reactivated during caldera collapse (early

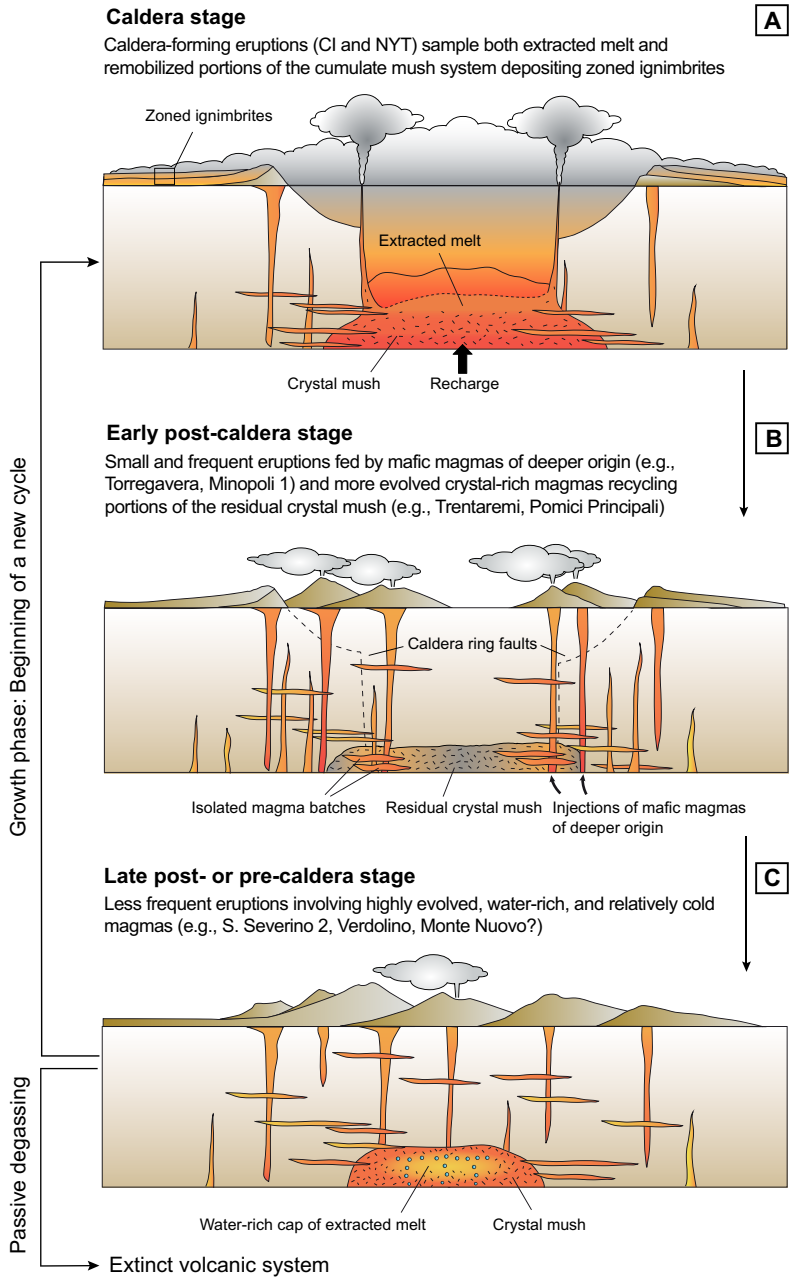

Fig. 5. Phases of a caldera cycle. (**A**) The caldera stage is characterized by large volume magma withdrawal involving the crystal-poor cap and part of the cumulate mush remobilized after more mafic recharge. This represents the main mechanisms responsible for the generation of gradients in the pyroclastic sequences of caldera-forming eruptions at Campi Flegrei (*27*, *28*). (**B**) The early post-caldera stage is associated with frequent injections of more mafic magmas of deeper origin into the upper crustal reservoir. Magmas can be erupted along the caldera ring faults or stall into the crust where they interact with the residual cumulate mush triggering remobilization and eruption of crystal-rich material. During this stage, eruption frequency is high and concentrates within the caldera. (**C**) The transition to the late post-caldera/pre-caldera stage is marked by a decrease of the eruption frequency, which allows magmas to stall in the crust and evolve via fractional crystallization. When the crystallinity of the system reaches ~50 to 70%, melt can be efficiently extracted from the crystal mush forming a crystal-poor and water-rich cap in the upper part of the reservoir (*32*). Modified after (*1*).

post-caldera stage; Fig. 5B). Some of these magmas injected at shallow crustal levels interacted with the residual cumulate crystal mush system, promoting remobilization and eruption of crystal-rich material (Fig. 5B). Indeed, at Campi Flegrei the post-caldera magmas (e.g., Trentaremi, Pomici Principali, and Astroni) record relatively high temperatures (Fig. 4), and the composition of mineral phases suggests crystal growth from an enriched melt derived via mixing of various proportions of high Ba-Sr-Mg recharge magmas and high Ba-Sr-Eu liquids derived from cumulate melting (Fig. 3 and fig. S3). However, the few positive Eu anomalies found in the composition of matrix glasses suggest that much smaller amounts of cumulate mush were melted compared to the caldera-forming eruptions (Fig. 2).

As time went on, the system was able to recuperate and started to regrow an upper crustal magma reservoir; some magma batches stalled in the crust and rebuilt a mush system capable of undergoing melt extraction (late post-caldera/pre-caldera stage; Fig. 5C). This stage was marked by eruption of highly evolved, crystal-poor, relatively cold, and water-rich magmas (e.g., S. Severino 1 and 2, Belvedere Milliscola 1 and 2, and Verdolino; Fig. 4). We suggest that the occurrence of magmas, with similar characteristics at different times after the NYT (Fondi di Baia and Averno 2; fig. S1) and particularly in the last eruption of Monte Nuovo, is an indication that a new pre-caldera phase of activity has started at Campi Flegrei.

Zooming in on the recent activity

An exceptionally rich stratigraphic and geochronological record is available for the post-NYT eruptive activity at Campi Flegrei caldera. More than 60 eruptions occurred during three epochs of almost continuous volcanic activity (~15 to 10.6 ka ago, ~9.6 to 9.1 ka ago, and ~5.5 to 3.5 ka ago) interrupted by three periods of dormancy marked by thick paleosols and unconformities correlated over the entire Campi Flegrei area (*18*, *20*, *37*). During each epoch, the eruption frequency was high, with recurrence intervals of few years to decades. The last eruption of Monte Nuovo (1538 AD) was isolated in time, occurring after a ~3 ka long period of quiescence (*20*).

Using this well-constrained stratigraphic framework, together with our new petrological data as input, we used a numerical model (*26*) to explore the thermomechanical evolution of the magma reservoir over the past 15 ka. The model allows tracking the evolution of physical parameters such as pressure, temperature, crystallinity, dissolved and exsolved water content, and reservoir volume. We adapted the model to conditions appropriate to Campi Flegrei using a phase diagram from thermodynamic modeling [rhyolite-MELTS (*38*); fig. S6] and a modified solubility curve for alkaline compositions based on experimental data from the literature [(*39*–*42*); fig. S7] to constrain the exsolution of the fluid phase. We defined initial and boundary conditions, as well as material properties, by testing the sensitivity of the results and the parameter uncertainty using scaling arguments in combination with the available petrologic, stratigraphic, and geochronological data (see Materials and Methods).

This analysis led to the model runs reported in table S1, among which run no. 1 best matches the natural behavior of the Campi Flegrei magmatic system over the past 15 ka (Fig. 6). Our model can reproduce the timing of eruption/dormancy when we set continuous recharge

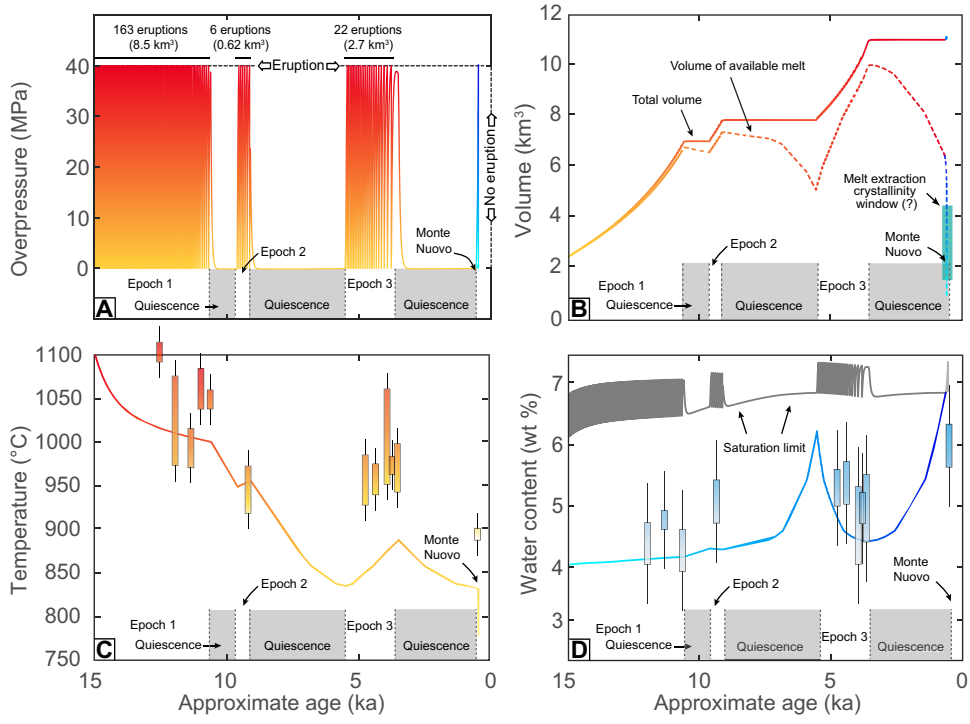

Fig. 6. Thermomechanical model. Variations of (**A**) overpressure (in MPa), (**B**) reservoir volume (in km^3), (**C**) temperature (in°C), and (**D**) water content (in wt %) over the past 15 ka at Campi Flegrei caldera obtained using thermomechanical modeling (*26*). In (A), eruption occurs when the critical overpressure reaches 40 MPa (*60*) and the magma is mobile [<50% crystals (*72*)]. The modeled number of eruptions and accumulated volumes (in km^3) are indicated for each eruptive epoch (see run no. 1 in table S1). In (B), the crystallinity window suitable for melt extraction is between 50 and 70% crystals (*32*). In (C) and (D), the equilibrium temperatures and magma water contents obtained by means of clinopyroxene-liquid thermometry and K-feldspar–liquid hygrometry, respectively (Fig. 4), are juxtaposed to the modeled curves for comparison. In (D), the gray curve refers to the H_2O saturation limit calculated on the basis of our refined solubility curve for alkaline compositions (fig. S7). See table S1 and figs. S8 and S9 for a comparison with other model results.

during the epochs of activity and no input during periods of quiescence (Fig. 6A). The total eruptible volume increases by a factor of ~4.5 over the past 15 ka from an initial chamber volume of 2.5 km^3, representing a small amount of melt leftover from the NYT eruption or accumulated from the mush shortly after the eruption (Fig. 6B). We suggest that, during epochs 1 to 3, magma water content was below saturation (i.e., no fluid phase was exsolved), consistent with findings for the Astroni eruption (epoch 3) (*43*). The absence of exsolved volatiles in a frequently replenished and small reservoir (≤10 km^3) favored high eruption frequency (*44*), as observed during epochs 1 to 3, with eruptions dominantly triggered by mafic recharge [e.g., Fondi di Baia (*45*), Agnano-M. Spina (*46*), Averno 2 (*29*), Astroni (*47*), and Nisida (*48*)]. Over time, the system progressively cooled, but this temperature trend was periodically hindered or inverted by recharge during the epochs (Fig. 6C). The last eruption of Monte Nuovo marked a critical change in the evolution of the system:

1) The magma water content reached saturation and started to exsolve fluids a few decades to centuries before eruption, as testified to the ground deformation pattern that preceded the Monte Nuovo event (*49*).

2) Crystallization was enhanced, as indicated by the nonlinear crystallinity versus temperature curve showing a sharp increase in crystallinity over a narrow temperature range, which coincides with the onset of feldspars crystallization (fig. S6).

3) The magma chamber entered in a mush state that provides optimal conditions for melt extraction [50 to 70% crystals (*32*); Fig. 6B].

This combination of exsolution and crystallization allows for a critical pressure build up in the reservoir that can lead to an eruption (*50*). In contrast to all previous post-NYT eruptions, the Monte Nuovo magmas do not record any petrological evidence of interaction with more mafic recharge. Hence, volatile exsolution induced by crystallization and cooling (i.e., second boiling) could be a potential trigger of the Monte Nuovo eruption (as it was for other pre-caldera events at Campi Flegrei when magmas with similar characteristics were erupted; see Figs. 1, 2, and 4).

The present state of affairs at Campi Flegrei

After the Monte Nuovo eruption, the Campi Flegrei caldera has entered a new phase of quiescence accompanied by several episodes of ground deformation. Three major periods of unrest characterized by shallow seismicity and an increase in hydrothermal degassing have been recorded since the 1950s, thus increasing concern for a potential reawakening (*22*). Transfer of magmatic fluids from the main reservoir located at a depth of 7 to 8 km to the shallow hydrothermal system (~3 km) has been indicated as the possible cause for the recent unrest (*23*). The high CO_2 content of fumarolic gases is compatible with the typical compositions of recharge magmas at Campi Flegrei [i.e., trachybasaltic (*23*)]. We suggest that this behavior is consistent with the presence of water-saturated conditions in the upper crustal phonolitic reservoir, which facilitates the accommodation of volatile-rich recharge magmas without leading to an eruption, promoting reservoir growth (*51*). Hence, we propose that the subvolcanic plumbing system at Campi Flegrei is currently entering a new build-up phase, potentially culminating, at some undetermined point in the future, in a large volume eruption.

MATERIALS AND METHODS

Analytical methods

Juvenile clasts representative of 23 different eruptions were sampled at Campi Flegrei caldera and in more distal outcrops (Fig. 1 and Supplementary Materials). All samples were analyzed for bulk rock composition by x-ray fluorescence (XRF) and inductively coupled plasma mass spectrometry (ICPMS) at Eidgenössische Technische Hochschule (ETH) Zürich. Fused whole-rock XRF beads (1:5 lithium tetraborate dilution) were analyzed using a PANalytical Axios wavelength-dispersive XRF spectrometer following a 2-hour devolatilization period at 950°C. Loss on ignition was calculated as the difference between the weight of the original sample (~1.6 g) and that of the sample after devolatilization. Subsequently, XRF pills were analyzed using a 193-nm Lambda Physik Excimer ArF laser coupled to a PerkinElmer ELAN 6100 ICPMS system. Analyses were calibrated and drift corrected using the NIST 610 synthetic glass standard and were blank corrected using a lithium tetraborate blank. Spot sizes were 90 μm (lithium tetraborate blank) and 40 μm (sample), and an average of three points was taken per sample. A subset of samples representative of all the studied eruptions was selected for glass, mineral chemistry, and crystallinity analyses. Mineral phases and matrix glass were analyzed for major elements by electron probe microanalysis (EPMA) at ETH Zürich and Istituto Nazionale di Geofisica e Vulcanologia (INGV) Rome. The operating conditions were as follows: 15-kV acceleration voltage, counting times of 20 s on the peaks and 10 s on the backgrounds, and 20 nA (clinopyroxene, feldspars, and oxides) or 15 nA (biotite and glass) beam current. To minimize alkali migration, K and Na were always measured first, and a defocused beam (20 μm) was used for feldspar, biotite, and glass analyses. Analyses were typically reproducible to <5% for all major and minor elements. Trace element compositions of mineral phases and matrix glass were measured by laser ablation ICPMS (LA-ICPMS) at ETH Zürich using a 193-nm ArF Excimer laser from Resonetics coupled to a Thermo Element XR ICPMS. A spot size of 43 μm was used for mineral analyses and reduced to 20 μm for glass analyses; output energy of the laser beam was typically ~3.5 J/cm^2. The MATLAB-based SILLS software (*52*) was used for data reduction using NIST 612 and NIST 610 external standards. The U.S. Geological Survey reference glass GSD-1G was used as a secondary standard to monitor the accuracy of the instrument. For each data point, appropriate major element concentrations from EPMA analyses were used as internal standards. Long-term laboratory reproducibility of homogeneous glass standards indicated precision significantly better than 5% for elements, whose concentration was much greater (i.e., 2×) than the detection limit. Relative crystallinity was estimated by means of x-ray powder diffraction at ETH Zürich using an AXS D8 Advance diffractometer equipped with a Lynxeye superspeed detector. Powdered samples were analyzed using CuKα radiation generated at 40 kV and 40 mA. Scans were run at 5° to 90° 2θ using a 0.02° step size and 1-s dwell time. Diffractograms were processed using the method described in (*27*). Both bulk rock and groundmass crystallinities were estimated for samples that showed incipient groundmass crystallization. In these cases, the relative crystallinity was calculated by subtraction. The full datasets of bulk rock, matrix glass, mineral chemistry, and crystallinity calculations are reported in data file S1.

Magma crystallization conditions

We estimated crystallization temperatures and magma water contents using a clinopyroxene-liquid thermometer (*24*) and a K-feldspar–liquid hygrometer (*25*) specifically calibrated to alkaline compositions akin to the Campi Flegrei magmas. We compared crystal cores with bulk rock/clinopyroxene-hosted melt inclusion compositions, which approximate the composition of the melt during the early stages of crystallization, and crystal rims with matrix glasses, which closely resemble the composition of residual melt during the final stages of crystal growth

(*53*). For the thermometric calculations, we used water contents of 3 wt % (mafic magmas, DI ≤ 73), 4 wt % (intermediate magmas, DI = 74 to 90), and 4.5 wt % (evolved magmas, DI ≥ 91). Notably, the estimated temperatures obtained by varying the water content by 2 wt % are included within the error of the method [±20°C; (*24*)]. A K-feldspar crystallization temperature of 850°C was used for the hygrometric calculation based on rhyolite-MELTS thermodynamic simulations (fig. S6). An error of ±0.7 wt % is normally associated with the magma water content estimated using this method (*25*). The equilibrium conditions between mineral and melt compositions were determined by means of test for equilibrium based on clinopyroxene-melt and K-feldspar–melt exchange reactions (*25*, *54*). Only equilibrium pairs were used for calculating temperatures and magma water contents. Note that a pressure input is required to account for the equilibrium between clinopyroxene and melt. We used 300 MPa for the most mafic magmas of Minopoli 1 and 2 (*55*, *56*), 250 MPa for the pre-CI and CI (*57*), and 200 MPa for all the other eruptions based on the most recent geophysical data (*58*), which identify the current melt storage zone at a depth of ~7.5 km, corresponding to ~200 MPa, assuming a density of about 2700 kg/m^3.

Thermomechanical modeling

We used the numerical model of (*26*) to calculate the thermomechanical evolution of a magma reservoir, accounting for magma recharge, crystallization, exsolution, cooling, viscous relaxation, and eruptions. In the model, the magma reservoir is assumed to consist of an eruptible portion, which we refer to as the magma chamber, surrounded by a colder, viscoelastic shell that represents a transition from the mush near the magma chamber to the crust far away from the chamber. We tracked the changes in pressure (P), temperature (T), volume (V), phase volume fractions ($\boldsymbol{\varepsilon}$), and densities ($\boldsymbol{\rho}$) of the magma chamber over time by solving a coupled set of ordinary differential equations. These equations were derived from the conservation of mass, water, and enthalpy in combination with relationships for the rate of volume change in the chamber and the rate of change of the melt and crystal density. The volume and density changes depend on the bulk moduli ($\boldsymbol{\beta}$) and thermal expansion coefficients of the respective phases. The former was varied between 3 ×10^9 and 12 ×10^9 Pa (table S1), and the latter was kept constant at 10^{-5} K^{-1}. In addition, the volume change of the chamber takes into account the viscoelastic deformation of the surrounding country rocks (*59*, *60*). We further added closure relationships for the density of the gas phase, and most importantly, the solubility of water and the melting curve that are appropriate for Campi Flegrei magmas. We referred to previous works (*26*, *44*) for a detailed description of the governing equations and focused here on the specific adaptation of the model to the case of Campi Flegrei.

The equation of state of the gas phase was parameterized from a modified Redlich-Kwong relationship and identical to the one used in (*26*). We adapted a phase diagram obtained through rhyolite-MELTS (fig. S6) using the bulk rock composition of sample VPa1 from the Pomici Principali eruption (epoch 1; see the Supplementary Materials). The initial water content was set at 4 wt %, the pressure at 200 MPa (see the "Magma crystallization conditions" section), and the oxygen fugacity at quartz-fayalite-magnetite buffer (QFM+1) (*61*). We assumed that intermediate magmas, akin to the Pomici Principali eruption, represent the starting compositions from which the most evolved magmas were derived via fractional crystallization in the upper crustal reservoir [depth, ~7.5 km (*58*)]; more mafic differentiation likely occurred deeper in the system. We set the latent heat of crystallization to 290 kJ/kg (*62*). We introduced a new parameterization for the solubility of water, m_{eq} in phonolitic melt using data from (*39*, *40*), [(*41*); MBP and LSP], and (*42*) (fig. S7)

$$m_{eq} = 10^{-2}\left(\begin{array}{c} P^{0.5}\left(13.34 - \dfrac{3.317\times10^4}{T} + \dfrac{2.072\times10^7}{T^2}\right) \\ +P\left(-2.108 + \dfrac{5286}{T} - \dfrac{3.227\times10^6}{T^2}\right) \\ +P^{1.5}\left(0.07972 - \dfrac{197.2}{T} + \dfrac{1.189\times10^5}{T^2}\right) \end{array}\right) \quad (1)$$

The form of the parameterization followed that of (*63*) for water in rhyolite. Note that, in Eq. 1, the units of pressure are in megapascal, temperature is in Kelvin, and H_2O is in weight %. The parameterization is valid for pressures ranging from 0 to 400 MPa and for temperatures between 973 and 1573 K. We set the latent heat of exsolution (vaporization) to a value of 610 kJ/kg (*62*).

For all the results in table S1, we used the following initial conditions for the magma chamber, consistent with the values used for the rhyolite-MELTS calculations: (i) Pressure was equal to the lithostatic pressure of 200 MPa; (ii) temperature was set at 1100°C; and (iii) water content was 4 wt % (undersaturated and no gas phase present). We used a melt and crystal density of 2400 kg/m^3. Because of the limited compressibility and the thermal expansion of the melt and crystal phases, their density was nearly constant (varied <1% within the calculations). The initial magma chamber volume was varied between 1.5 and 5 km^3 (table S1).

Imposing a set of boundary conditions completed the model description. A sphere sitting in a larger spherical shell describes the heat loss from the magma chamber. The inner sphere has the temperature of the magma chamber. The larger shell has 10 times the radius of the initial magma chamber. We set a fixed temperature at the edge of the outer shell. For this value, we explored a range between 231° and 262°C (table S1), corresponding to a geothermal gradient of about 31° to 35°C/km in the far field, which is typical for volcanic regions. The effective viscosity of the crustal shell was calculated from the temperature profile between the magma chamber and the outer shell, as described in (*26*). Its initial value, η_{r0}, ranges between ~1 × 10^{18} and 7 × 10^{18} Pa s, with the lowest value corresponding to the hottest outer boundary and vice versa (table S1). It evolves over time toward roughly double the initial value during a single calculation. A new magma was injected in the magma chamber during the time intervals that correspond to the eruptive epochs (i.e., 15 to 10.6 ka ago, 9.6 to 9.1 ka ago, and 5.5 to 3.5 ka ago). The rate of injection was varied between 1.5 × 10^{-3} and 6 × 10^{-3} km^3/year during these periods and was set to zero in the periods of quiescence. The injected magma has a temperature of 1100°C and a water content of 4 wt %.

An eruption that results in mass removal from the magma chamber starts when a critical overpressure $(\Delta P)_c$ is reached. The eruption will cease when the lithostatic background pressure is reached as it is difficult to keep a conduit to the surface open under these conditions (i.e., it would collapse under the force of the surrounding crust). The critical overpressure is subject to relatively large uncertainties. The value of the critical overpressure has been suggested to be anywhere between 1 and 100 MPa (*64*–*67*). However, based on the scaling in (*60*, *67*), a value between 20 and 80 MPa is reasonable for a dyke to propagate and reach the surface without solidifying. We explored the effect of changing the value of critical overpressure within this range on our model results in the Supplementary Materials. In addition, the magma

needs to be mobile for an eruption to occur, and thus, its crystallinity needs to be below the critical fraction at which jamming occurs. The critical crystallinity is also not tightly constrained, as the ability of a crystalline magma to flow depends on several variables that influence magma rheology (*68*). It typically ranges between 40 and 60%, and we used a value of 50% in this study. See the Supplementary Materials for additional discussion on scaling, sensitivity, and caveats of the model.

SUPPLEMENTARY MATERIALS

Supplementary material for this article is available at http://advances.sciencemag.org/cgi/content/full/4/11/eaat9401/DC1

Fig. S1. Variation of the DI (DI = Q + Ab + Or + Ne + Lc normative) with time at Campi Flegrei.
Fig. S2. Geochemistry of volcanic rocks from Campi Flegrei.
Fig. S3. Clinopyroxene compositions.
Fig. S4. Plagioclase compositions.
Fig. S5. Biotite compositions.
Fig. S6. Melting curve.
Fig. S7. Solubility curve.
Fig. S8. Effect of varying critical overpressure on the model results.
Fig. S9. Effect of varying recharge rate on the model results.
Table S1. Compilation of literature data and model runs.
Data file S1. Tables reporting sample list, bulk rock and matrix glass analyses, mineral chemistry, and crystallinity of the sampled units.
References (*73*–*100*)

REFERENCES AND NOTES

1. P. W. Lipman, The roots of ash flow calderas in Western North-America: Windows into the tops of granitic batholiths. *J. Geophys. Res.* **89**, 8801–8841 (1984).
2. O. Bachmann, C. D. Deering, J. S. Ruprecht, C. Huber, A. Skopelitis, C. Schnyder, Evolution of silicic magmas in the Kos-Nisyros volcanic center, Greece: A petrological cycle associated with caldera collapse. *Contrib. Mineral. Petrol.* **163**, 151–166 (2011).
3. A. Rubin, K. M. Cooper, M. Leever, J. Wimpenny, C. Deering, T. Rooney, D. Gravley, Q.-Z. Yin, Changes in magma storage conditions following caldera collapse at Okataina Volcanic Center, New Zealand. *Contrib. Mineral. Petrol.* **171**, 4 (2016).
4. B. A. Óladóttir, O. Sigmarsson, G. Larsen, T. Thordarson, Katla volcano, Iceland: Magma composition, dynamics and eruption frequency as recorded by Holocene tephra layers. *Bull. Volcanol.* **70**, 475–493 (2008).
5. J. A. Wolff, J. N. Gardner, Is the Valles caldera entering a new cycle of activity? *Geology* **23**, 411–414 (1995).
6. T. H. Druitt, M. Mercier, L. Florentin, E. Deloule, N. Cluzel, T. Flaherty, E. Médard, A. Cadoux, Magma storage and extraction associated with plinian and interplinian activity at Santorini Caldera (Greece). *J. Petrol.* **57**, 461–494 (2016).
7. T. H. Druitt, R. S. J. Sparks, On the formation of Calderas during ignimbrite eruptions. *Nature* **310**, 679–681 (1984).
8. L. Civetta, G. Orsi, L. Pappalardo, R. V. Fisher, G. Heiken, M. Ort, Geochemical zoning, mingling, eruptive dynamics and depositional processes—The Campanian Ignimbrite, Campi Flegrei caldera, Italy. *J. Volcanol. Geotherm. Res.* **75**, 183–219 (1997).
9. O. Bachmann, G. W. Bergantz, Rejuvenation of the Fish Canyon magma body: A window into the evolution of large-volume silicic magma systems. *Geology* **31**, 789–792 (2003).
10. W. Hildreth, Volcanological perspectives on Long Valley, Mammoth Mountain, and Mono Craters: Several contiguous but discrete systems. *J. Volcanol. Geotherm. Res.* **136**, 169–198 (2004).
11. J. A. Vazquez, M. R. Reid, Time scales of magma storage and differentiation of voluminous high-silica rhyolites at Yellowstone caldera, Wyoming. *Contrib. Mineral. Petrol.* **144**, 274–285 (2002).
12. M. R. Rampino, S. Self, Volcanic winter and accelerated glaciation following the Toba super-eruption. *Nature* **359**, 50–52 (1992).
13. C. Scarpati, P. Cole, A. Perrotta, The Neapolitan Yellow Tuff—A large volume multiphase eruption from Campi Flegrei, Southern Italy. *Bull. Volcanol.* **55**, 343–356 (1993).
14. B. De Vivo, G. Rolandi, P. B. Gans, A. Calvert, W. A. Bohrson, F. J. Spera, H. E. Belkin, New constraints on the pyroclastic eruptive history of the Campanian volcanic Plain (Italy). *Miner. Petrol.* **73**, 47–65 (2001).
15. L. Pappalardo, M. Piochi, M. D'Antonio, L. Civetta, R. Petrini, Evidence for multi-stage magmatic evolution during the past 60 kyr at Campi Flegrei (Italy) deduced from Sr, Nd and Pb isotope data. *J. Petrol.* **43**, 1415–1434 (2002).
16. A. L. Deino, G. Orsi, S. de Vita, M. Piochi, The age of the Neapolitan Yellow Tuff caldera-forming eruption (Campi Flegrei caldera Italy) assessed by $^{40}Ar/^{39}Ar$ dating method. *J. Volcanol. Geotherm. Res.* **133**, 157–170 (2004).
17. L. Fedele, C. Scarpati, M. Lanphere, L. Melluso, V. Morra, A. Perrotta, G. Ricci, The Breccia Museo formation, Campi Flegrei, southern Italy: Geochronology, chemostratigraphy and relationship with the Campanian Ignimbrite eruption. *Bull. Volcanol.* **70**, 1189–1219 (2008).
18. R. Isaia, P. Marianelli, A. Sbrana, Caldera unrest prior to intense volcanism in Campi Flegrei (Italy) at 4.0 ka B.P.: Implications for caldera dynamics and future eruptive scenarios. *Geophys. Res. Lett.* **36**, L21303 (2009).
19. M. Piochi, G. Mastrolorenzo, L. Pappalardo, Magma ascent and eruptive processes from textural and compositional features of Monte Nuovo pyroclastic products, Campi Flegrei, Italy. *Bull. Volcanol.* **67**, 663–678 (2005).
20. V. C. Smith, R. Isaia, N. J. G. Pearce, Tephrostratigraphy and glass compositions of post-15 kyr Campi Flegrei eruptions: Implications for eruption history and chronostratigraphic markers. *Quat. Sci. Rev.* **30**, 3638–3660 (2011).
21. G. Orsi, S. DeVita, M. di Vito, The restless, resurgent Campi Flegrei nested caldera (Italy): Constraints on its evolution and configuration. *J. Volcanol. Geotherm. Res.* **74**, 179–214 (1996).
22. C. R. J. Kilburn, G. De Natale, S. Carlino, Progressive approach to eruption at Campi Flegrei caldera in southern Italy. *Nat. Commun.* **8**, 15312 (2017).
23. G. Chiodini, A. Paonita, A. Aiuppa, A. Costa, S. Caliro, P. De Martino, V. Acocella, J. Vandemeulebrouck, Magmas near the critical degassing pressure drive volcanic unrest towards a critical state. *Nat. Commun.* **7**, 13712 (2016).
24. M. Masotta, S. Mollo, C. Freda, M. Gaeta, G. Moore, Clinopyroxene–liquid thermometers and barometers specific to alkaline differentiated magmas. *Contrib. Mineral. Petrol.* **166**, 1545–1561 (2013).
25. S. Mollo, M. Masotta, F. Forni, O. Bachmann, G. De Astis, G. Moore, P. Scarlato, A K-feldspar–liquid hygrometer specific to alkaline differentiated magmas. *Chem. Geol.* **392**, 1–8 (2015).
26. W. Degruyter, C. Huber, A model for eruption frequency of upper crustal silicic magma chambers. *Earth Planet. Sci. Lett.* **403**, 117–130 (2014).
27. F. Forni, O. Bachmann, S. Mollo, G. De Astis, S. E. Gelman, B. S. Ellis, The origin of a zoned ignimbrite: Insights into the Campanian Ignimbrite magma chamber (Campi Flegrei, Italy). *Earth Planet. Sci. Lett.* **449**, 259–271 (2016).
28. F. Forni, E. Petricca, O. Bachmann, S. Mollo, G. De Astis, M. Piochi, The role of magma mixing/mingling and cumulate melting in the Neapolitan Yellow Tuff caldera-forming eruption (Campi Flegrei, Southern Italy). *Contrib. Mineral. Petrol.* **173**, 10.1007/s00410-018-1471-4 (2018).
29. C. Fourmentraux, N. Métrich, A. Bertagnini, M. Rosi, Crystal fractionation, magma step ascent, and syn-eruptive mingling: The Averno 2 eruption (Phlegraean Fields, Italy). *Contrib. Mineral. Petrol.* **163**, 1121–1137 (2012).
30. M. D'Antonio, L. Civetta, P. Di Girolamo, Mantle source heterogeneity in the Campanian Region (South Italy) as inferred from geochemical and isotopic features of mafic volcanic rocks with shoshonitic affinity. *Miner. Petrol.* **67**, 163–192 (1999).
31. M. D'Antonio, Lithology of the basement underlying the Campi Flegrei caldera: Volcanological and petrological constraints. *J. Volcanol. Geotherm. Res.* **200**, 91–98 (2011).
32. J. Dufek, O. Bachmann, Quantum magmatism: Magmatic compositional gaps generated by melt-crystal dynamics. *Geology* **38**, 687–690 (2010).
33. A. Parmigiani, S. Faroughi, C. Huber, O. Bachmann, Y. Su, Bubble accumulation and its role in the evolution of magma reservoirs in the upper crust. *Nature* **532**, 492–495 (2016).
34. J. A. Wolff, B. S. Ellis, F. C. Ramos, W. A. Starkel, S. Boroughs, P. H. Olin, O. Bachmann, Remelting of cumulates as a process for producing chemical zoning in silicic tuffs: A comparison of cool, wet and hot, dry rhyolitic magma systems. *Lithos* **236–237**, 275–286 (2015).
35. S. E. Gelman, C. D. Deering, O. Bachmann, C. Huber, F. J. Gutiérrez, Identifying the crystal graveyards remaining after large silicic eruptions. *Earth Planet. Sci. Lett.* **403**, 299–306 (2014).
36. R. S. J. Sparks, L. A. Marshall, Thermal and mechanical constraints on mixing between mafic and silicic magmas. *J. Volcanol. Geotherm. Res.* **29**, 99–124 (1986).
37. M. A. Di Vito, R. Isaia, G. Orsi, J. Southon, S. de Vita, M. D'Antonio, L. Pappalardo, M. Piochi, Volcanism and deformation since 12,000 years at the Campi Flegrei caldera (Italy). *J. Volcanol. Geotherm. Res.* **91**, 221–246 (1999).
38. G. A. R. Gualda, M. S. Ghiorso, R. V. Lemons, T. L. Carley, Rhyolite-MELTS: A modified calibration of MELTS optimized for silica-rich, fluid-bearing magmatic systems. *J. Petrol.* **53**, 875–890 (2012).
39. M. R. Carroll, J. G. Blank, The solubility of H_2O in phonolitic melts. *Am. Mineral.* **82**, 549–556 (1997).
40. J. D. Webster, B. Goldoff, M. F. Sintoni, N. Shimizu, B. De Vivo, C-O-H-Cl-S-F volatile solubilities, partitioning, and mixing in phonolitic-trachytic melts and aqueous-carbonic vapor saline liquid at 200 MPa. *J. Petrol.* **55**, 2217–2247 (2014).
41. B. C. Schmidt, H. Behrens, Water solubility in phonolite melts: Influence of melt composition and temperature. *Chem. Geol.* **256**, 259–268 (2008).
42. D. B. Dingwell, D. M. Harris, C. M. Scarfe, The solubility of H_2O in melts in the system SiO_2-Al_2O_3-Na_2O-K_2o at 1 to 2 Kbars. *J. Geol.* **92**, 387–395 (1984).

43. M. J. Stock, M. C. S. Humphreys, V. C. Smith, R. Isaia, D. M. Pyle, Late-stage volatile saturation as a potential trigger for explosive volcanic eruptions. *Nat. Geosci.* **9**, 249–290 (2016).
44. W. Degruyter, C. Huber, O. Bachmann, K. M. Cooper, A. J. R. Kent, Magma reservoir response to transient recharge events: The case of Santorini volcano (Greece). *Geology* **44**, 23–26 (2016).
45. M. Pistolesi, A. Bertagnini, A. Di Roberto, R. Isaia, A. Vona, R. Cioni, G. Giordano, The Baia–Fondi di Baia eruption at Campi Flegrei: Stratigraphy and dynamics of a multi-stage caldera reactivation event. *Bull. Volcanol.* **79**, 67 (2017).
46. R. S. Iovine, L. Fedele, F. C. Mazzeo, I. Arienzo, A. Cavallo, G. Wörner, G. Orsi, L. Civetta, M. D'Antonio, Timescales of magmatic processes prior to the ~4.7 ka Agnano-Monte Spina eruption (Campi Flegrei caldera, Southern Italy) based on diffusion chronometry from sanidine phenocrysts. *Bull. Volcanol.* **79**, 18 (2017).
47. S. Tonarini, M. D'Antonio, M. A. Di Vito, G. Orsi, A. Carandente, Geochemical and B–Sr–Nd isotopic evidence for mingling and mixing processes in the magmatic system that fed the Astroni volcano (4.1–3.8 ka) within the Campi Flegrei caldera (southern Italy). *Lithos* **107**, 135–151 (2009).
48. I. Arienzo, F. C. Mazzeo, R. Moretti, A. Cavallo, M. D'Antonio, Open-system magma evolution and fluid transfer at Campi Flegrei caldera (Southern Italy) during the past 5 ka as revealed by geochemical and isotopic data: The example of the Nisida eruption. *Chem. Geol.* **427**, 109–124 (2016).
49. M. A. Di Vito, V. Acocella, G. Aiello, D. Barra, M. Battaglia, A. Carandente, C. D. Gaudio, S. de Vita, G. P. Ricciardi, C. Ricco, R. Scandone, F. Terrasi, Magma transfer at Campi Flegrei caldera (Italy) before the 1538 AD eruption. *Sci. Rep.* **6**, 32245 (2016).
50. S. Tramontano, G. A. R. Gualda, M. S. Ghiorso, Internal triggering of volcanic eruptions: Tracking overpressure regimes for giant magma bodies. *Earth Planet. Sci. Lett.* **472**, 142–151 (2017).
51. H. E. Huppert, A. W. Woods, The role of volatiles in magma chamber dynamics. *Nature* **420**, 493–495 (2002).
52. M. Guillong, D. L. Meier, M. M. Allan, C. A. Heinrich, B. W. D. Yardley, SILLS: A MATLAB-based program for the reduction of laser ablation ICP-MS data of homogeneous materials and inclusions. *Short Course Notes - Geol. Assoc. Can.* **40**, 328–333 (2008).
53. K. D. Putirka, Thermometers and barometers for volcanic systems. *Rev. Mineral. Geochem.* **69**, 61–120 (2008).
54. S. Mollo, M. Masotta, Optimizing pre-eruptive temperature estimates in thermally and chemically zoned magma chambers. *Chem. Geol.* **368**, 97–103 (2014).
55. C. Cannatelli, A. Lima, R. J. Bodnar, B. De Vivo, J. D. Webster, L. Fedele, Geochemistry of melt inclusions from the Fondo Riccio and Minopoli 1 eruptions at Campi Flegrei (Italy). *Chem. Geol.* **237**, 418–432 (2007).
56. A. Mangiacapra, R. Moretti, M. Rutherford, L. Civetta, G. Orsi, P. Papale, The deep magmatic system of the Campi Flegrei caldera (Italy). *Geophys. Res. Lett.* **35**, 10.1029/2008GL035550 (2008).
57. L. Pappalardo, L. Ottolini, G. Mastrolorenzo, The Campanian Ignimbrite (southern Italy) geochemical zoning: Insight on the generation of a super-eruption from catastrophic differentiation and fast withdrawal. *Contrib. Mineral. Petrol.* **156**, 1–26 (2008).
58. A. Zollo, N. Maercklin, M. Vassallo, D. Dello Iacono, J. Virieux, P. Gasparini, Seismic reflections reveal a massive melt layer feeding Campi Flegrei caldera. *Geophys. Res. Lett.* **35**, 10.1029/2008GL034242 (2008).
59. M. Dragoni, C. Magnanensi, Displacement and stress produced by a pressurized, spherical magma chamber, surrounded by a viscoelastic shell. *Phys. Earth Planet. Inter.* **56**, 316–328 (1989).
60. A. M. Jellinek, D. J. DePaolo, A model for the origin of large silicic magma chambers: Precursors of caldera-forming eruptions. *Bull. Volcanol.* **65**, 363–381 (2003).
61. W. A. Bohrson, F. J. Spera, S. J. Fowler, H. E. Belkin, B. De Vivo, G. Rolandi, Petrogenesis of the Campanian Ignimbrite: Implications for crystal-melt separation and open-system processes from major and trace elements and Th isotopic data. *Dev. Volcanol.* **9**, 249–288 (2006).
62. L. Caricchi, J. Blundy, Experimental petrology of monotonous intermediate magmas. *Geol. Soc. Spec. Publ.* **422**, 105–130 (2015).
63. J. Dufek, G. W. Bergantz, Lower crustal magma genesis and preservation: A stochastic framework for the evaluation of basalt–crust interaction. *J. Petrol.* **46**, 2167–2195 (2005).
64. E. B. Grosfils, Magma reservoir failure on the terrestrial planets: Assessing the importance of gravitational loading in simple elastic models. *J. Volcanol. Geotherm. Res.* **166**, 47–75 (2007).
65. E. B. Grosfils, P. J. McGovern, P. M. Gregg, G. A. Galgana, D. M. Hurwitz, S. M. Long, S. R. Chestler, Elastic models of magma reservoir mechanics: A key tool for investigating planetary volcanism, in *Volcanism and Tectonism across the Inner Solar System*, T. Platz, M. Massironi, P. K. Byrne, H. Hiesinger, Eds. (Geological Society, London, Special Publication, 2015), pp. 239–267, vol. 401.
66. A. Gudmundsson, Magma chambers: Formation, local stresses, excess pressures, and compartments. *J. Volcanol. Geotherm. Res.* **237**, 19–41 (2012).
67. A. M. Rubin, Propagation of magma-filled cracks. *Annu. Rev. Earth Planet. Sci.* **23**, 287–336 (1995).
68. H. M. Mader, E. W. Llewellin, S. P. Mueller, The rheology of two-phase magmas: A review and analysis. *J. Volcanol. Geotherm. Res.* **257**, 135–158 (2013).
69. G. De Natale, C. Troise, D. Mark, A. Mormone, M. Piochi, M. A. Di Vito, R. Isaia, S. Carlino, D. Barra, R. Somma, The Campi Flegrei Deep Drilling Project (CFDDP): New insight on caldera structure, evolution and hazard implications for the Naples area (Southern Italy). *Geochem. Geophys. Geosyst.* **17**, 4836–4847 (2016).
70. S. Vitale, R. Isaia, Fractures and faults in volcanic rocks (Campi Flegrei, southern Italy): Insight into volcano-tectonic processes. *Int. J. Earth Sci.* **103**, 801–819 (2014).
71. W. F. McDonough, S.-s. Sun, The composition of the Earth. *Chem. Geol.* **120**, 223–253 (1995).
72. C. Huber, O. Bachmann, J. Dufek, Crystal-poor versus crystal-rich ignimbrites: A competition between stirring and reactivation. *Geology* **40**, 115–118 (2012).
73. C. Scarpati, A. Perrotta, S. Lepore, A. Calvert, Eruptive history of Neapolitan volcanoes: Constraints from ^{40}Ar-^{39}Ar dating. *Geol. Mag.* **150**, 412–425 (2013).
74. C. D'Oriano, E. Poggianti, A. Bertagnini, R. Cioni, P. Landi, M. Polacci, M. Rosi, Changes in eruptive style during the AD 1538 Monte Nuovo eruption (Phlegrean Fields, Italy): The role of syn-eruptive crystallization. *Bull. Volcanol.* **67**, 601–621 (2005).
75. M. A. Di Vito, I. Arienzo, G. Braia, L. Civetta, M. D'Antonio, V. Di Renzo, G. Orsi, The Averno 2 fissure eruption: A recent small-size explosive event at the Campi Flegrei Caldera (Italy). *Bull. Volcanol.* **73**, 295–320 (2011).
76. J. T. Sliwinski, B. S. Ellis, P. Dávila-Harris, J. A. Wolff, P. H. Olin, O. Bachmann, The use of biotite trace element compositions for fingerprinting magma batches at Las Cañadas volcano, Tenerife. *Bull. Volcanol.* **79**, 1 (2017).
77. L. Caricchi, C. Annen, J. Blundy, G. Simpson, V. Pinel, Frequency and magnitude of volcanic eruptions controlled by magma injection and buoyancy. *Nat. Geosci.* **7**, 126–130 (2014).
78. W. J. Malfait, R. Seifert, S. Petitgirard, J.-P. Perrillat, M. Mezouar, T. Ota, E. Nakamura, P. Lerch, C. Sanchez-Valle, Supervolcano eruptions driven by melt buoyancy in large silicic magma chambers. *Nat. Geosci.* **7**, 122–125 (2014).
79. O. Karakas, W. Degruyter, O. Bachmann, J. Dufek, Lifetime and size of shallow magma bodies controlled by crustal-scale magmatism. *Nat. Geosci.* **10**, 446–450 (2017).
80. L. Karlstrom, S. R. Paterson, A. M. Jellinek, A reverse energy cascade for crustal magma transport. *Nat. Geosci.* **10**, 604–608 (2017).
81. M. Fedi, F. Cella, M. D'Antonio, G. Florio, V. Paoletti, V. Morra, Gravity modeling finds a large magma body in the deep crust below the Gulf of Naples, Italy. *Sci. Rep.* **8**, 8229 (2018).
82. L. Karlstrom, H. M. Wright, C. R. Bacon, The effect of pressurized magma chamber growth on melt migration and pre-caldera vent locations through time at Mount Mazama, Crater Lake, Oregon. *Earth Planet. Sci. Lett.* **412**, 209–219 (2015).
83. L. Karlstrom, J. Dufek, M. Manga, Magma chamber stability in arc and continental crust. *J. Volcanol. Geotherm. Res.* **190**, 249–270 (2010).
84. S. Pabst, G. Wörner, L. Civetta, R. Tesoro, Magma chamber evolution prior to the Campanian Ignimbrite and Neapolitan Yellow Tuff eruptions (Campi Flegrei, Italy). *Bull. Volcanol.* **70**, 961–976 (2008).
85. B. S. Ellis, O. Bachmann, J. A. Wolff, Cumulate fragments in silicic ignimbrites: The case of the Snake River Plain. *Geology* **42**, 431–434 (2014).
86. F. Bégué, C. D. Deering, D. M. Gravley, B. M. Kennedy, I. Chambefort, G. A. R. Gualda, O. Bachmann, Extraction, storage and eruption of multiple isolated magma batches in the paired Mamaku and Ohakuri Eruption, Taupo Volcanic Zone, New Zealand. *J. Petrol.* **55**, 1653–1684 (2014).
87. J. Blundy, K. V. Cashman, A. Rust, F. Witham, A case for CO_2-rich arc magmas. *Earth Planet. Sci. Lett.* **290**, 289–301 (2010).
88. O. Bachmann, G. W. Bergantz, Gas percolation in upper-crustal silicic crystal mushes as a mechanism for upward heat advection and rejuvenation of near-solidus magma bodies. *J. Volcanol. Geotherm. Res.* **149**, 85–102 (2006).
89. J. Mungall, Physical Controls of Nucleation, Growth and Migration of Vapor Bubbles in Partially Molten Cumulates, in *Layered Intrusions. Springer Geology*, B. Charlier, O. Namur, R. Latypov, C. Tegner, Eds. (Springer, 2015).
90. A. Parmigiani, W. Degruyter, S. Leclaire, C. Huber, O. Bachmann, The mechanics of shallow magma reservoir outgassing. *Geochem. Geophys. Geosyst.* **18**, 2887–2905 (2017).
91. L. Melluso, V. Morra, A. Perrotta, C. Scarpati, M. Adabbo, The eruption of the Breccia Museo (Campi-Flegrei, Italy); Fractional crystallization processes in a shallow, zoned magma chamber and implications for the eruptive dynamics. *J. Volcanol. Geotherm. Res.* **68**, 325–339 (1995).
92. G. Orsi, L. Civetta, M. Dantonio, P. Digirolamo, M. Piochi, Step-filling and development of a 3-layer magma chamber - the neapolitan-yellow-tuff case-history. *J. Volcanol. Geotherm. Res.* **67**, 291–312 (1995).
93. K. Wohletz, G. Orsi, S. Devita, Eruptive mechanisms of the neapolitan-yellow-tuff interpreted from stratigraphic, chemical, and granulometric data. *J. Volcanol. Geotherm. Res.* **67**, 263–290 (1995).
94. L. Pappalardo, L. Civetta, M. D'Antonio, A. Deino, M. Di Vito, G. Orsi, A. Carandente, S. de Vita, R. Isaia, M. Piochi, Chemical and Sr-isotopical evolution of the Phlegraean

magmatic system before the Campanian Ignimbrite and the Neapolitan Yellow Tuff eruptions. *J. Volcanol. Geotherm. Res.* **91**, 141–166 (1999).
95. S. Signorelli, G. Vaggelli, L. Francalanci, M. Rosi, Origin of magmas feeding the Plinian phase of the Campanian Ignimbrite eruption, Phlegrean Fields (Italy): Constraints based on matrix-glass and glass-inclusion compositions. *J. Volcanol. Geotherm. Res.* **91**, 199–220 (1999).
96. M. Polacci, L. Pioli, M. Rosi, The Plinian phase of the Campanian Ignimbrite eruption (Phlegrean Fields, Italy): Evidence from density measurements and textural characterization of pumice. *Bull. Volcanol.* **65**, 418–432 (2003).
97. P. Fulignati, P. Marianelli, M. Proto, A. Sbrana, Evidences for disruption of a crystallizing front in a magma chamber during caldera collapse: An example from the Breccia Museo unit (Campanian Ignimbrite eruption, Italy). *J. Volcanol. Geotherm. Res.* **133**, 141–155 (2004).
98. P. Marianelli, A. Sbrana, M. Proto, Magma chamber of the Campi Flegrei supervolcano at the time of eruption of the Campanian Ignimbrite. *Geology* **34**, 937–940 (2006).
99. I. Arienzo, L. Civetta, A. Heumann, G. Wörner, G. Orsi, Isotopic evidence for open system processes within the Campanian Ignimbrite (Campi Flegrei–Italy) magma chamber. *Bull. Volcanol.* **71**, 285–300 (2009).
100. L. Melluso, R. De'Gennaro, L. Fedele, L. Franciosi, V. Morra, Evidence of crystallization in residual, Cl–F-rich, agpaitic, trachyphonolitic magmas and primitive Mg-rich basalt–trachyphonolite interaction in the lava domes of the Phlegrean Fields (Italy). *Geol. Mag.* **149**, 532–550 (2012).

Acknowledgments: We are grateful to L. Martin and M. Guillong for the assistance during EPMA and LA-ICPMS analyses. G. Gualda and three anonymous referees are thanked for constructive reviews and C.-T. Lee for the editorial work. **Funding:** This project was supported by Swiss National Science Foundation grant 200021_146268 to O.B. **Author contribution:** F.F. and O.B. are responsible for the petrological part. W.D. developed the numerical model and adapted it to the Campi Flegrei conditions. S.M. contributed to estimate the temperatures and water contents of magmas. G.D.A. is responsible for the sampling and stratigraphic correlations. All authors contributed to the interpretation of the data and to the writing of the manuscript, with F.F. taking the lead. **Competing interests:** The authors declare that they have no competing interests. **Data and materials availability:** All data needed to evaluate the conclusions in the paper are present in the paper and/or the Supplementary Materials. The complete dataset that supports the findings of this study is available in data file S1. Additional data related to this paper may be requested from the authors.

Submitted 21 April 2018
Accepted 12 October 2018
Published 14 November 2018
10.1126/sciadv.aat9401

Citation: F. Forni, W. Degruyter, O. Bachmann, G. De Astis, S. Mollo, Long-term magmatic evolution reveals the beginning of a new caldera cycle at Campi Flegrei. *Sci. Adv.* **4**, eaat9401 (2018).

Science Advances

Long-term magmatic evolution reveals the beginning of a new caldera cycle at Campi Flegrei

Francesca Forni, Wim Degruyter, Olivier Bachmann, Gianfilippo De Astis and Silvio Mollo

Sci Adv **4** (11), eaat9401.
DOI: 10.1126/sciadv.aat9401